Proc. NIPR Symp. Upper Atmos. Phys., 1, 99–109, 1988

THERMOSPHERIC STRUCTURE ASSOCIATED WITH DISCRETE LEVELS OF AURORAL ACTIVITY

Sawako MAEDA[1]*, Timothy J. FULLER-ROWELL[2] and Dave S. EVANS[3]

[1]*CIRES, University of Colorado, Boulder, CO 80309, U.S.A.*
[2]*University College London, Gower Street, London, WC1E 6BT, U.K.*
[3]*SEL, NOAA, Boulder, CO 80303, U.S.A.*

Abstract: A time-dependent calculation has been done to study dynamical and compositional structure of the thermosphere associated with discrete levels of auroral activity. The auroral activity level is given in terms of estimates of hemispheric power input due to particle precipitations. Heat and momentum input originated from the magnetosphere is estimated by using an empirical model constructed from the two data bases of the precipitating particles monitored by the TIROS/NOAA satellites and the ionospheric convection electric field measured by the Millstone Hill Incoherent Scatter Radar. The main results are summarized as follows: At the level of moderate auroral activity, the horizontal and vertical winds are very weak. High-latitude heating is in the same order of magnitude as the solar EUV/UV heating. These two heatings cause a temperature minimum at mid-latitudes. The latitudinal variation of the mean molecular mass is small. At the highest level of auroral activity, the strong equatorward wind is excited associated with the high-latitude upward wind. A temperature bulge appears at high latitudes and the mean molecular mass increases due to the upwelling of the molecular-rich air. The dynamical response to the auroral activity is faster than the thermal and compositional response. The thermal response depends significantly on the radiative cooling by nitric oxide.

1. Introduction

The dynamics and composition of the neutral thermosphere are strongly coupled to the magnetospheric/ionospheric processes. Energetic particles precipitating from the magnetosphere cause ionization of the neutral gas at the ionospheric heights. The ion-electron pairs produced deposit the heat energy through the various processes such as charge exchange and dissociative recombination. In addition to these atomistic processes, the combination of the increase in conductivity by the ionization and the ionospheric convection electric field provides the heat energy for the neutral gas due to the Joule dissipation of the electric currents. The convection electric field also provides the neutral gas the momentum via ion-drag.

Modeling of the response of the global thermosphere to the high-latitude energy input has been extensively done (MAYR and VOLLAND, 1974; FULLER-ROWELL and REES, 1981; ROBLE *et al.*, 1982; ROBLE and KASTING, 1984). In these models, the ion convection and particle precipitation were described in an ideal manner. The

* Present address: Osaka College, Hirao, Mihara, Minamikawachi, Osaka 587.

energy input associated with the magnetospheric/ionospheric processes is, however, largely variable in space and time compared to the heating due to the absorption of solar EUV and UV radiation. In order to represent a large variability of high-latitude energy input, an empirical model has been developed by utilizing the TIROS/NOAA particle measurements and the observations of the ionospheric convection electric field by the Millstone Hill Incoherent Scatter Radar (FOSTER *et al.*, 1986; FULLER-ROWELL and EVANS, 1987). In that model, all the parameters which govern the high-latitude energy input are given as a function of auroral activity level. The measurements of particle energy flux by the TIROS/NOAA satellites have also been used to estimate the total amount of particle energy delivered to an entire auroral hemisphere. These estimates of hemispheric power input play a role of an activity index (FOSTER *et al.*, 1986; FULLER-ROWELL and EVANS, 1987).

The model of high-latitude energy input has been used as the driving input to a time-dependent calculation of the thermospheric response to the changes in the high-latitude energy input. The purpose of this paper is to study the characteristics of the thermospheric response to discrete levels of auroral activities. A numerical simulation model of the zonally-averaged thermosphere is used, originating from the nested grid model of FULLER-ROWELL (1984). The model solves the momentum, energy, continuity and three constituent composition equations of the neutral gas self-consistently under the assumption of hydrostatic equilibrium.

Although the relative concentration of the neutral major species (N_2, O_2 and O) is calculated consistently with temperature and neutral wind, the ion composition is fixed and not updated consistently with the neutral concentration. Once initial height profiles of minor neutral species such as N(^{2}D), N(^{4}S) and NO are obtained by taking account the odd nitrogen chemistry, these profiles are fixed in the following time-dependent calculation. As discussed by ROBLE and EMERY (1983), the radiative cooling by NO is very important for the heat budget of the thermosphere. The NO density enhancement at geomagnetic disturbances is estimated by using an empirical formula of CRAVENS (1981). His formula that expresses the number density of NO as a function of the *Kp*-index with 9 h time delay is converted to be a function of the TIROS/NOAA activity index. The statistical relationship between *Kp* and the auroral power index was used to convert the Cravens' formula.

2. Model

The latitudinal grid extends between the geographic poles in 5 degree increments. The vertical grid covers 16 scale heights starting from the fixed lower boundary located at 70 km height. A time step is set to be 30 s. The pole values of winds, temperature and composition are taken as the extrapolation of the closest three points on the same pressure level. At the lower boundary, the neutral velocity is zero and the temperature is fixed to be 220 K. The pressure at the lower boundary is taken as 5.2285 Pa. At the upper boundary the vertical gradients of velocity and temperature are assumed to be zero. The vertical velocity on a constant pressure level is zero. At the lower boundary, the photochemical equilibrium is assumed between O_2 and O, and the mass mixing ratio of N_2 is fixed to be 0.77. At the upper levels, the diffusive equilibrium is

assumed.

To initialize the two-dimensional arrays, initial one-dimensional steady state profiles of temperature and composition are required. This was achieved by integrating the composition and energy equation for 30 days simulation time with all horizontal gradients set to be zero. All the results presented in this paper are appropriate for the conditions of the low solar activity ($F_{10.7}=80\times10^{-22}$ W/cm^2/s) and equinox. The profiles of zonally-averaged solar heating rate and three kinds of the radiative cooling rates by O, CO_2 and NO are shown in Fig. 1. The resultant initial temperature profile and the profiles for the three major constituents and the odd nitrogen minor constituents are shown in Figs. 2 and 3, respectively. It is noted here that the 'log pressure' shown on the vertical axis is $-2\log(p/p_0)$, meaning that log pressure 2, for example, corresponds to the pressure level one scale height higher than the lower boundary.

The total ion number density is defined as the square root of the sum of the squares of solar produced ionization and that produced by the particle precipitation. The solar produced ionization is evaluated from an ionospheric model of CHIU (1975). The ion-neutral collision frequency and the Hall and Pedersen conductivities are given by an expression of SCHUNK and WALKER (1973).

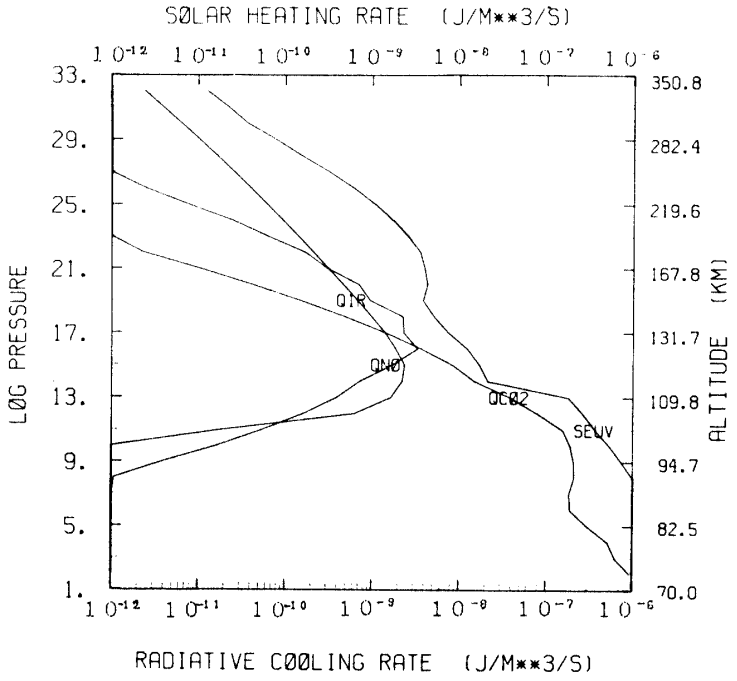

Fig. 1. Initial profiles of solar heating rate (SEUV) and radiative cooling rates by O (QIR), NO (QNO) and CO_2 (QCO_2) used in our model.

Zonal averages of the Hall and Pedersen conductivities given over the geographic latitude and log pressure grid are shown in Figs. 4 and 5 for the two activity levels 5 and 9. They do not include the solar contribution. The level 5 corresponds to a moderate auroral activity, the level 9 a very strong activity. The peak magnitude of the Hall conductivity is 8×10^{-5} and 64×10^{-5} mhos/m for the two levels, respectively. As for the Pedersen conductivity, they are 4×10^{-5} and 34×10^{-5} mhos/m, respectively.

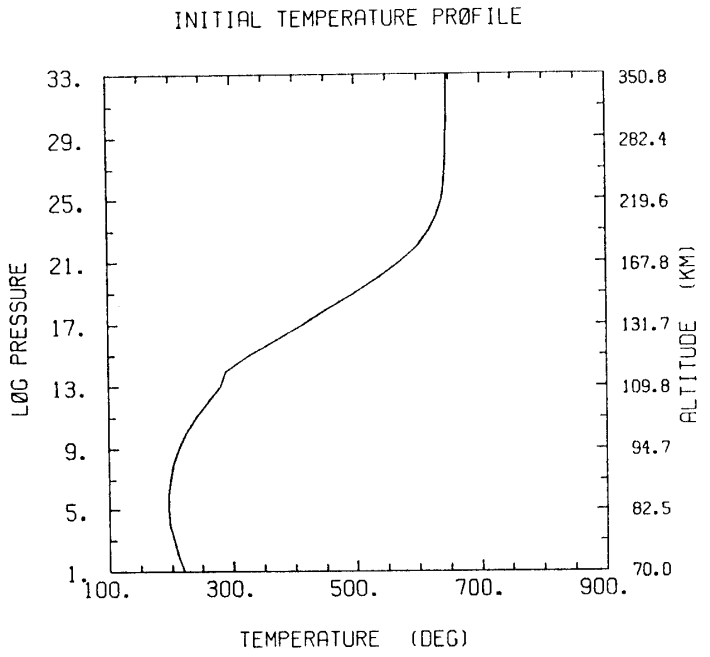

Fig. 2. Initial profile of temperature used in our model.

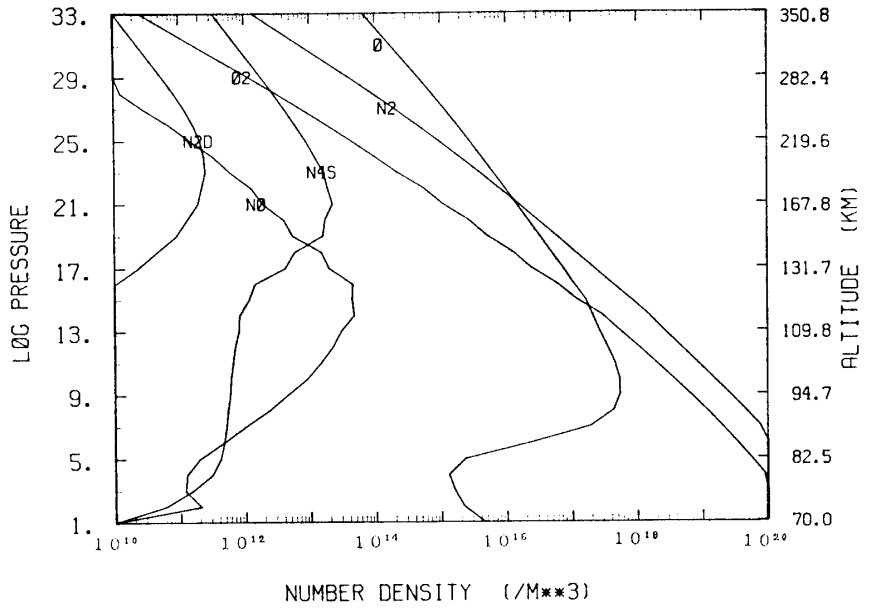

Fig. 3. Initial profiles of neutral constituents (O, N_2, O_2, NO, $N(^2D)$ and $N(^4S)$) used in our model.

It can easily be seen that the peak altitude of the Hall conductivity is lower than that of the Pedersen conductivity.

The particle heating rate given by the energy loss per ion-electron pair takes the value of 35 eV (REES, 1963). The height-dependent heating efficiency derived by REES *et al.* (1983) was used. The zonal averages of the particle heating rate per unit mass are shown in Fig. 6 for the two activity levels. The peak magnitude is 2 and 6 J/kg/s for the two levels, respectively. In comparison with the solar heating rate

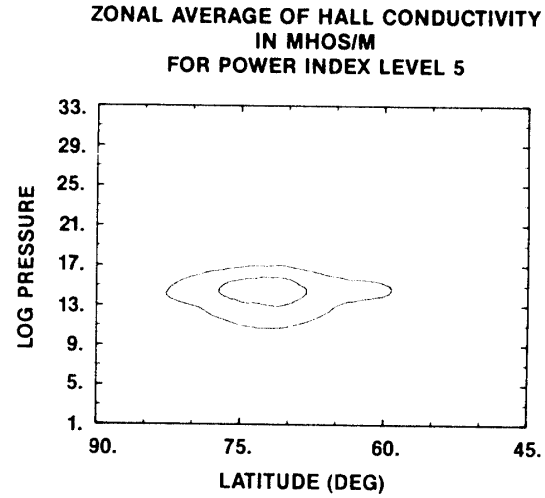

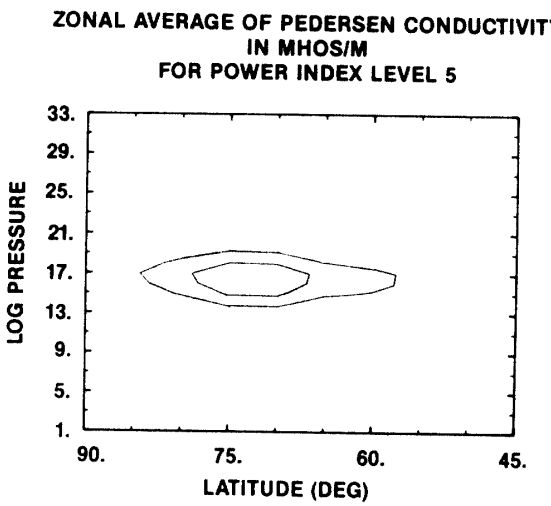

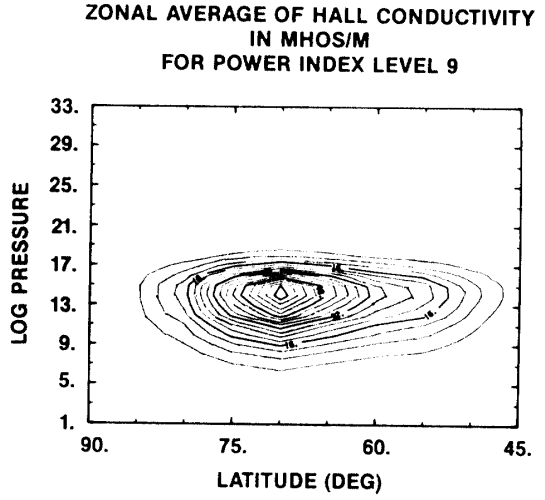

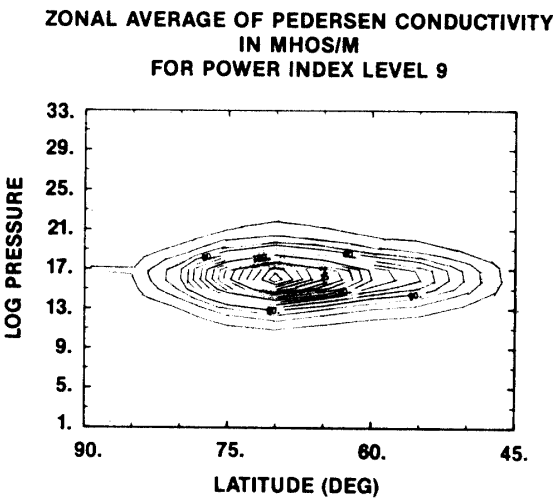

Fig. 4. Zonal average of Hall conductivity given over the geographic latitude and log pressure grid for the activity levels 5 and 9. Units are 10^{-5} mhos/m, with a contour spacing of 4×10^{-5} mhos/m.

Fig. 5. Same as Fig. 4, except for the Pedersen conductivity. Units are 10^{-6} mhos/m, with a contour spacing of 2×10^{-5} mhos/m.

shown in Fig. 1, it can be inferred that the particle heating is at maximum near the peak altitude of the solar heating but the magnitude of the particle heating rate is less than that of the solar heating rate. In order to estimate the Joule heating rate, knowledge of the neutral winds existing at the ionospheric altitudes is required. The Joule heating rate, that was computed after each time step self-consistently with the neutral winds, would be shown later.

3. Results and Discussions

In this paper, a simulation has been done to investigate the characteristics of the thermospheric structure associated with a moderate auroral activity (level 5) and with a strong activity (level 9). A modeled time variation of the auroral activity was as follows: for the first 24 h, the activity level continued to be constant (5 or 9), and

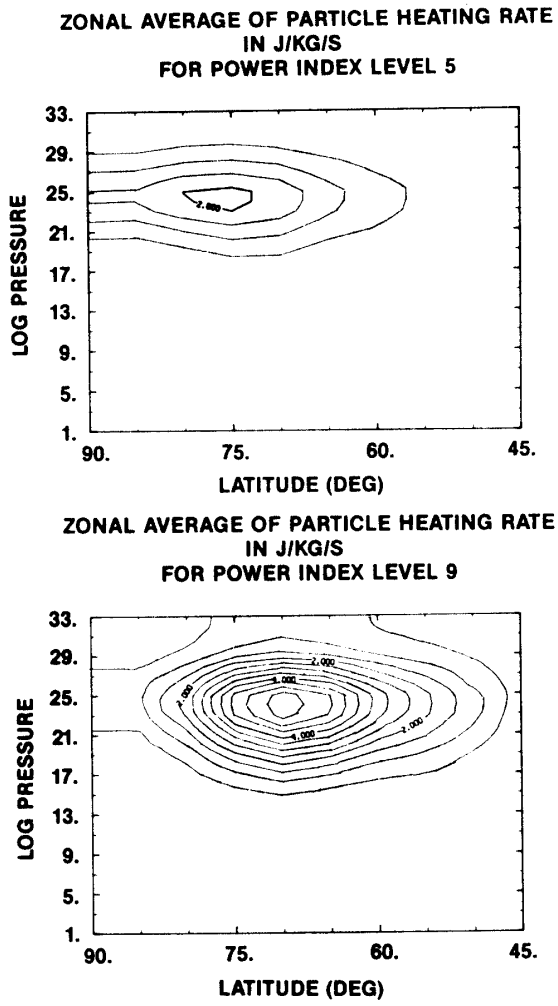

Fig. 6. Same as Fig. 4, except for the particle heating rate. Units are J/kg/s, with a contour spacing of 0.5 J/kg/s.

then it went down to be the lowest level of 1. Figure 7 shows the thermospheric response on a constant pressure level observed at 70° and 45° latitudes in the case of the activity level 9. The long duration of high activity level represents a strong, major geomagnetic storm. The assumed activity level is given the bottom of Fig. 7. The altitude of the pressure level chosen here increased from 334 to 430 km at 60° latitude. The pressure level was lifted up by 100 km due to a thermal expansion of the atmosphere. The third curves show the time variation of the temperature during the period. The temperature rapidly increased in response to the storm activity. The temperature increase at the high latitude of 70° was about 600 K and even at mid-latitude of 45° it was about 300 K. After the activity subsided, the temperature recovered slowly with a decay time of about a day. Even if the heat energy is poured into the atmosphere at a constant rate, the temperature increase achieved for every 3 h tends to cease and the temperature seems to approach asymptotically to a constant value. It seems likely that for the long duration of the high auroral activity, the enhanced radiative cooling by NO supresses the temperature increase.

The dynamical response was largely different from the thermal response. The initial poleward wind was turned to the equatorward wind very quickly. The new wind field was established promptly in response to the high-latitude heating.

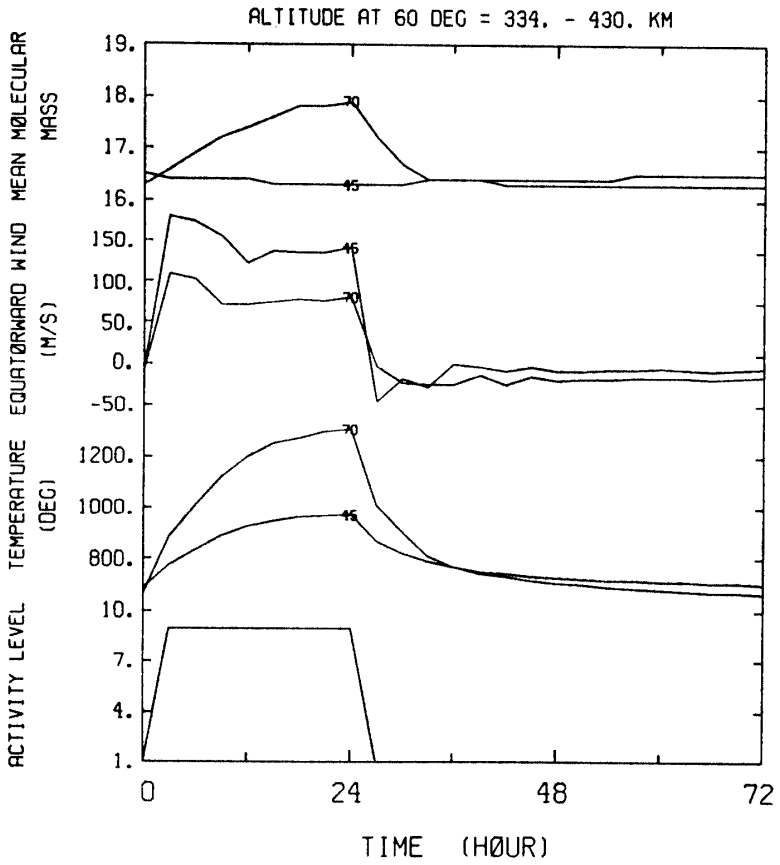

Fig. 7. Time histories of the calculated temperature, meridional wind and mean molecular mass on a constant pressure level at latitudes of 70° and 45°. The pressure level chosen here is 334 km height at the initial time and lifted up to 430 km at 24 h simulation time. The time history of the activity level is shown at the bottom.

The time variation in the mean molecular mass evaluated from the relative constituents of the three major species was shown by the top curves in Fig. 7. In the region of high-latitude heating, the molecular-rich air replaced the air above it and the mean molecular mass increased with time. Outside the heating region, the mean molecular mass slightly decreased. The time variation of the mean molecular mass was similar to the temperature variation.

From the time variation shown in Fig. 7, it can be inferred that the thermosphere approaches to an equilibrium under a few days duration of auroral activity with a constant level. The snap shots taken at 24 h simulation time given in Figs. 8–10 could represent 'quasi-steady state' structures associated with constant activity levels. Figure 8 is the zonally averaged Joule heating rate for the levels of 5 and 9. The latitudinal range taken here is from the equator to the pole. The symmetry with respect to the equator was assumed. The height level corresponding to a constant pressure level at the latitude of 45° is shown on the right ordinate. The peak magnitudes of the Joule heating rate were 10 and 90 J/kg/s for the levels 5 and 9, respectively. They are much greater than those of the particle heating rate. The Joule heating is maximized at the upper pressure level than the particle heating. Therefore, the effect of the Joule heating on the thermospheric dynamics is much greater than the

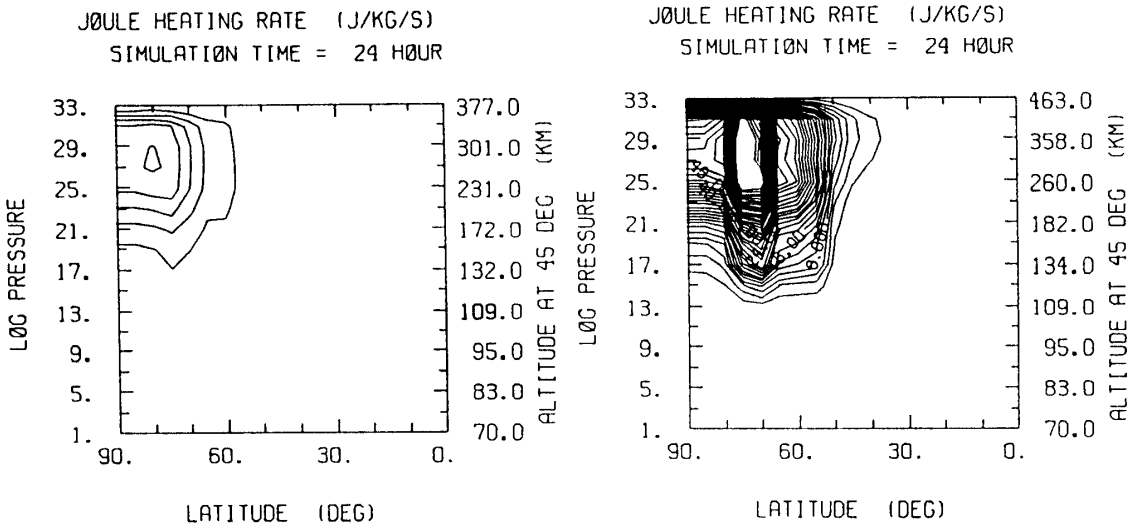

Fig. 8. Contour maps of the Joule heating rate at 24 h simulation time in the cases of the activity level 5 (left) and 9 (right). Units are J/kg/s, with a contour spacing of 2 J/kg/s.

effect of the particle heating. The sum of the particle and Joule heating rates at the level 5 is almost the same order of magnitude as the solar heating rate, but the latter dominates at low latitudes.

The contour maps of the meridional and vertical winds are shown in Fig. 9. At the activity level 5, the high-latitude heating was balanced with the solar heating and the meridional wind was very weak. The high-latitude heating at the level 9 excited the strong upward wind up to 7 m/s accompanied by the equatorward wind. The peak velocity of the equatorward wind was 173 m/s. A weak downward wind appeared at mid-latitudes. The vertical wind plotted on the constant pressure levels includes the component induced by the horizontally diverging winds on the pressure levels and the component caused by the thermal expansion of the atmosphere. The top boundary with the activity level 9 was higher than that with the level 5 by about 90 km owing to the thermal expansion.

Figure 10 shows the spatial distribution of the temperature and the mean molecular mass. The temperature above 200 km height varied greately with the activity level. The temperature below 150 km, however, was not affected by the high-latitude heating. Without the high-latitude heating, the warmest temperature appeared over the equator because the solar heating rate at the equator is greater than that at the pole. When the activity level was moderate, there appeared a temperature minimum at mid-latitudes. The weak high-latitude heating caused the temperature enhancement over the polar region. A temperature bulge at high-latitudes developed as the activity level increased. Even at low-latitudes, the exospheric temperature was 1000 K. The contour maps of the mean molecular mass visualize the upwelling of the molecular-rich air during the disturbed period. The composition change at high-latitudes is primarily caused by an upward wind due to the local heating. The composition change at mid-latitudes is, however, due to a weak downward wind induced by the horizontally diverging winds on the pressure surface.

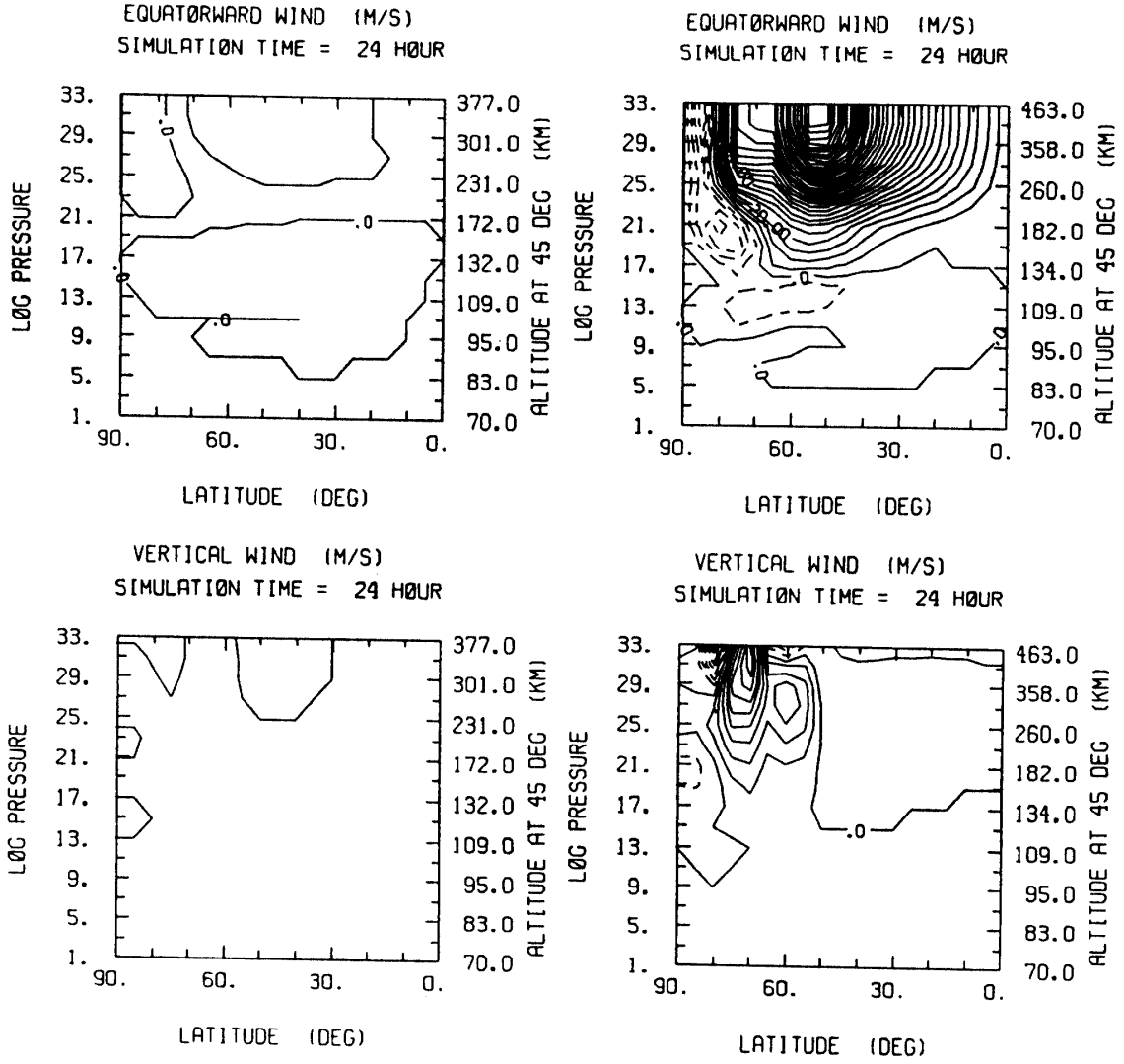

Fig. 9. Same as Fig. 8, except for the meridional and vertical winds. Units are m/s, with a contour spacing of 5 m/s for the meridional wind and 1 m/s for the vertical wind.

In order to estimate the characteristic time of the thermospheric response to the auroral activity, it is very important to evaluate the radiative cooling rate self-consistently with temperature and composition. Without the enhancement of NO density during the auroral activity, not shown here, the relaxiation time of temperature is much longer than that shown in Fig. 7. As was already discussed in Section 1, the minor neutral constituents were not updated consistently with the major constituents, and the enhancement of the NO density was estimated in an approximate way. Eventually, the continuity equation for NO should be solved self-consistently with solar and auroral particle production via the dissociation of molecular nitrogen.

Acknowledgments

The first two authors are grateful to the Cooperative Institute for Research in the Environmental Sciences at the University of Colorado for their stay at the Space En-

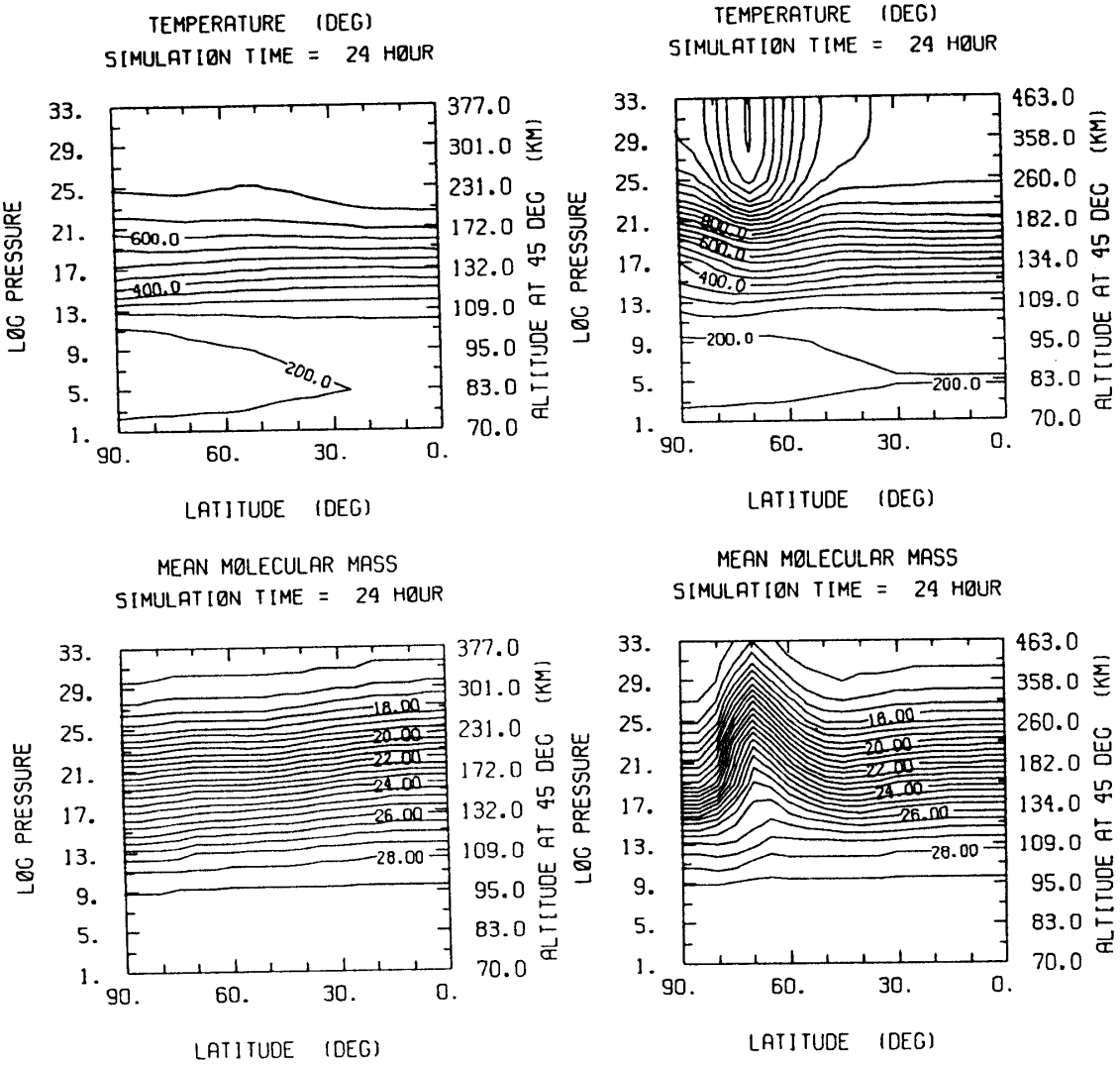

Fig. 10. Same as Fig. 8, except for the temperature and mean molecular mass.

vironment Laboratory, NOAA.

References

CHIU, Y. T. (1975): An improved phenomenological model of ionospheric density. J. Atmos. Terr. Phys., **37**, 1563–1570.

CRAVENS, T. E. (1981): The global distribution of nitric oxide at 200 km. J. Geophys. Res., **86**, 5710–5714.

FOSTER, J. C., HOLT, J. M., MUSGROVE, R. G. and EVANS, D. S. (1986): Ionospheric convection associated with discrete levels of particle precipitation. Geophys. Res. Lett., **13**, 656–659.

FULLER-ROWELL, T. J. (1984): A two-dimensional, high-resolution, nested-grid model of the thermosphere. J. Geophys. Res., **89**, 2971–2990.

FULLER-ROWELL, T. J. and EVANS, D. S. (1987): Height integrated Pedersen and Hall conductivity patterns inferred from the TIROS/NOAA satellite data. J. Geophys. Res., **92**, 7606–7618.

FULLER-ROWELL, T. J. and REES, D. (1981): A three-dimensional, time-dependent simulation of the global dynamical response of the thermosphere to a geomagnetic substorm. J. Atmos. Terr. Phys., **43**, 701–721.

MAYR, H. G. and VOLLAND, H. (1974): Magnetic storm dynamics of the thermosphere. J. Atmos. Terr. Phys., **36**, 2025–2036.

REES, M. H. (1963): Auroral ionization and excitation by incident energetic electrons. Planet. Space Sci., **11**, 1209–1218.

REES, M. H., EMERY, B. A., ROBLE, R. G. and STAMNES, K. (1983): Neutral and ion gas heating by auroral electron precipitation. J. Geophys. Res., **88**, 6289–6300.

ROBLE, R. G. and EMERY, B. A. (1983): On the global mean temperature of the thermosphere. Planet. Space Sci., **31**, 597–614.

ROBLE, R. G. and KASTING, J. F. (1984): The zonally averaged circulation, temperature, and compositional structure of the lower thermosphere and variations with geomagnetic activity. J. Geophys. Res., **89**, 1711–1724.

ROBLE, R. G., DICKINSON, R. E. and RIDLEY, E. C. (1982): Global circulation and temperature structure of thermosphere with high-latitude plasma convection. J. Geophys. Res., **87**, 1599–1614.

SCHUNK, R. W. and WALKER, J. C. G. (1973): Theoretical ion densities in the lower ionosphere. Planet. Space Sci., **21**, 1875–1896.

(Received May 11, 1987; Revised manuscript received September 7, 1987)